Cellular Microbiology (2011) **13**(7), 1026–1043
doi:10.1111/j.1462-5822.2011.01600.x
First published online 26 Apr 2011

Pore-forming toxins induce multiple cellular responses promoting survival

Manuel R. Gonzalez,[1] Mirko Bischofberger,[1] Barbara Frêche,[1] Sylvia Ho,[1] Robert G. Parton[2] and F. Gisou van der Goot[1]*

[1]*Global Health Institute, Ecole Polytechnique Fédérale de Lausanne, Faculty of Life Sciences, Station 15, CH 1015 Lausanne, Switzerland.*

[2]*University of Queensland, Institute for Molecular Bioscience, Brisbane, Qld 4072, Australia.*

Summary

Pore-forming toxins (PFTs) are secreted proteins that contribute to the virulence of a great variety of bacterial pathogens. They inflict one of the more disastrous damages a target cell can be exposed to: disruption of plasma membrane integrity. Since this is an ancient form of attack, which bares similarities to mechanical membrane damage, cells have evolved response pathways to these perturbations. Here, it is reported that PFTs trigger very diverse yet specific response pathways. Many are triggered by the decrease in cytoplasmic potassium, which thus emerges as a central regulator. Upon plasma membrane damage, cells activate signalling pathways aimed at restoring plasma membrane integrity and ion homeostasis. Interestingly these pathways do not require protein synthesis. Cells also trigger signalling cascades that allow them to enter a quiescent-like state, where minimal energy is consumed while waiting for plasma membrane damage to be repaired. More specifically, protein synthesis is arrested, cytosolic constituents are recycled by autophagy and energy is stored in lipid droplets.

Introduction

Bacteria have developed an arsenal of tools to affect crucial cellular functions of the host, allowing them to manipulate the cells' behaviour to their own benefit. The first bacterial weapons to be identified were protein toxins, since these are soluble proteins secreted by the pathogen into the extracellular medium and thus more amenable to investigation than intracellular virulence factors. Among toxins, the most widely spread group is that of pore-forming toxins (PFTs), which composes some 25% of all known bacterial protein toxins (Iacovache *et al.*, 2008; Bischofberger *et al.*, 2009). Interestingly, the ability to produce pore-forming proteins has been kept during evolution and PFTs can be found in amoeba, worms and plants (Gonzalez *et al.*, 2008) and even in humans, as recently illustrated by the similarity between PFTs and perforin (Hadders *et al.*, 2007; Rosado *et al.*, 2007).

Exposure to high doses of PFTs leads to cell death, which can be either apoptotic, necrotic (Bhakdi and Tranum-Jensen, 1991; Nelson *et al.*, 1999; Golstein and Kroemer, 2007; Kennedy *et al.*, 2009) or for immune cells, through pyroptosis (Kepp *et al.*, 2010). The more recently emerging view is however that during infection, many cells are actually exposed to sublytic doses of PFTs and under such conditions have the capacity to respond to the insult (reviewed in Aroian and van der Goot, 2007; Bischofberger *et al.*, 2009) and possibly even warn other cells of the attack (Yarovinsky *et al.*, 2008). The hypothesis that cells respond is supported by several recent studies showing that exposure to a PFT can lead to the activation of signalling pathways such as the NF-κB pathway, the p38 MAPK pathway, the inflammasome, the Unfolded Protein Response, inhibition of SUMOylation, dephosphorylation of histones and autophagy (Walev *et al.*, 1994; Chopra *et al.*, 2000; Huffman *et al.*, 2004; Gurcel *et al.*, 2006; Husmann *et al.*, 2006; Ratner *et al.*, 2006; Hamon *et al.*, 2007; Bischof *et al.*, 2008; Aguilar *et al.*, 2009; Bellier *et al.*, 2009; Kloft *et al.*, 2009; Mestre *et al.*, 2010; Meyer-Morse *et al.*, 2010; Ribet *et al.*, 2010). The exact role of these pathways in cellular responses has generally not been evaluated. Moreover, most studies were performed looking at a single pathway, on a given cell type, for a given toxin and it is therefore not clear how general these findings are and whether all pathways are equally important for all toxins.

The ability of a cell to cope with pore formation indeed depends on one hand on the type of cell – for example immune, epithelial or fibroblast cells – and on the other on the type of PFT and the nature/abundance of its surface receptors (see below, for review on PFTs see Iacovache *et al.*, 2008), its concentration and the time of exposure.

Received 17 February, 2011; accepted 16 March, 2011. *For correspondence. E-mail gisou.vandergoot@epfl.ch; Tel. (+41) 21 693 1791; Fax (+41) 21 693 9538.

Our interest was to study, in parallel, two PFTs that differ greatly: aerolysin and listeriolysin O (LLO). Aerolysin, produced by *Aeromonas hydrophila*, forms heptameric pores of 1.5–2 nm in diameter (Abrami *et al*., 2000). LLO, produced by *Listeria monocytogenes*, which was chosen as a representative of the cholesterol-dependent cytolysin (CDC) family, forms pores of variable stoichiometry – up to 50mers – with diameters reaching 30 nm (Gilbert, 2010; Heuck *et al*., 2010). In correlation with the pore diameters, aerolysin pores have a conductance of ≈ 400 pS (Iacovache *et al*., 2006), while those formed by CDCs may exceed 1 nS (Korchev *et al*., 1998). These two toxins also differ in terms of identity and abundance of their receptors. While aerolysin binds to GPI-anchored proteins (Abrami *et al*., 2000), cholesterol is thought to be the receptor for various CDCs (Gilbert, 2010; Heuck *et al*., 2010). Finally, the stability of the pores formed by these two toxins differs. The aerolysin heptamer is immensely stable (Lesieur *et al*., 1999), reminiscent of prion aggregates, while CDC oligomers are SDS-sensitive (Shepard *et al*., 2000).

We first investigated, using a panel of assays, the effect of these toxins on plasma membrane integrity of a human intestinal epithelial cell line, a physiological target of both of these toxins. We established conditions for each toxin at which cells recover from the challenge. Using phosphoarrays, we found that both toxins robustly and specifically activate MAP kinase pathways and show that the ERK and p38 pathways contribute to the recovery of ion homeostasis.

Since we found that recovery of plasma membrane integrity requires from 1 h – for LLO – to 8 h – for aerolysin, at the population level, we wondered whether, during that time, cells would undergo a toxin-triggered transition to a quiescent-like state, reminiscent of the G0 state in yeast that allows cells to survive during nutrient starvation (Gray *et al*., 2004). We found that PFTs not only trigger autophagy, as observed by others (Gutierrez *et al*., 2007; Kloft *et al*., 2010; Mestre *et al*., 2010; Meyer-Morse *et al*., 2010), but also a transient arrest in protein synthesis and formation of lipid droplets, two phenomena also observed in the G0 state of yeast. Remarkably, none of these three processes occurred when toxin-induced potassium efflux was prevented, a treatment that also blocked the PFT-induced activation of p38 and Erk.

Altogether our work shows (i) that despite the differences between the two toxins, both trigger similar signalling cascades, albeit with different kinetics, (ii) that cellular potassium is a master regulator of the response to PFTs, and (iii) that cells trigger different categories of responses, some promoting recovery of membrane integrity, others transition to a low-energy-consumption state, in addition to the previously described inflammatory responses and changes in gene transcription.

Results

Effect of aerolysin and LLO on intracellular potassium concentrations

Since both aerolysin and LLO are known to act in the intestine during food-borne infections by *Aeromonas* and *Listeria*, respectively, the intestinal cell line, HT29, was chosen as the target cell type of most experiments. When HT29 cells were exposed to proaerolysin [10 ng ml^{-1} ≈ 0.19 nM, proaerolysin is the aerolysin precursor form that is processed by cell surface proteases to aerolysin (Abrami *et al*., 1998a)], their intracellular potassium levels rapidly dropped and remained low over time (Fig. 1A). However when HT29 cells were exposed to proaerolysin for only 60 min (here after called PA^{pulse}) and subsequently incubated in a toxin-free medium, the potassium drop was followed by a slow recovery to normal levels after 8–10 h. There was no detectable cell growth during this time period (Fig. S1A). Even when cells were exposed only 5 min to proaerolysin, cellular potassium levels still drop and the recovery still required more than 6 h (not shown). The recovery following PA^{pulse} was not due to the entry of intracellular calcium, as observed during repair of mechanical plasma membrane injury (McNeil and Steinhardt, 2003) (Fig. S1B). The fact that recovery is slow following a PA^{pulse} is not due to the fact that PA rather that the proteolytically processed aerolysin was added to the cells. Indeed no cellular recovery was observed upon transient exposure to 10 ng ml^{-1} aerolysin – obtained by *in vitro* proteolysis of proaerolysin – possibly because the cells cannot cope with a more synchronized wave of pore formation (not shown). Recovery was only observed with lower concentrations of aerolysin. Unless specified, in all subsequent studies using aerolysin, cells were exposed to a 1 h pulse of proaerolysin.

Exposure of HT29 cells to LLO (500 ng ml^{-1} ≈ 8.5 nM) led to a more rapid and even more pronounced drop in intracellular potassium. Cells however replenished their potassium pool within less than 2 h, a process that could be accelerated by removing LLO from the medium after 10 min (Fig. 1B). Recover of cellular potassium was ATP-dependent (not shown). Extracellular calcium was not essential since recovery was also observed following a 10 min LLO pulse in an EGTA containing medium (Fig. S1C). Cellular potassium however failed to recovery in the presence of EGTA when cells were continuously exposed to LLO (not shown), indicating that extracellular calcium is required during prolonged exposure to LLO, in agreement with previous findings on the related toxin streptolysin O (Walev *et al*., 2001).

In all subsequent experiments, cells were exposed to LLO continuously, in contrast to proaerolysin where 1 h pulses were used. It has been documented that LLO is rapidly inactivated at neutral pH (Schuerch *et al*., 2005),

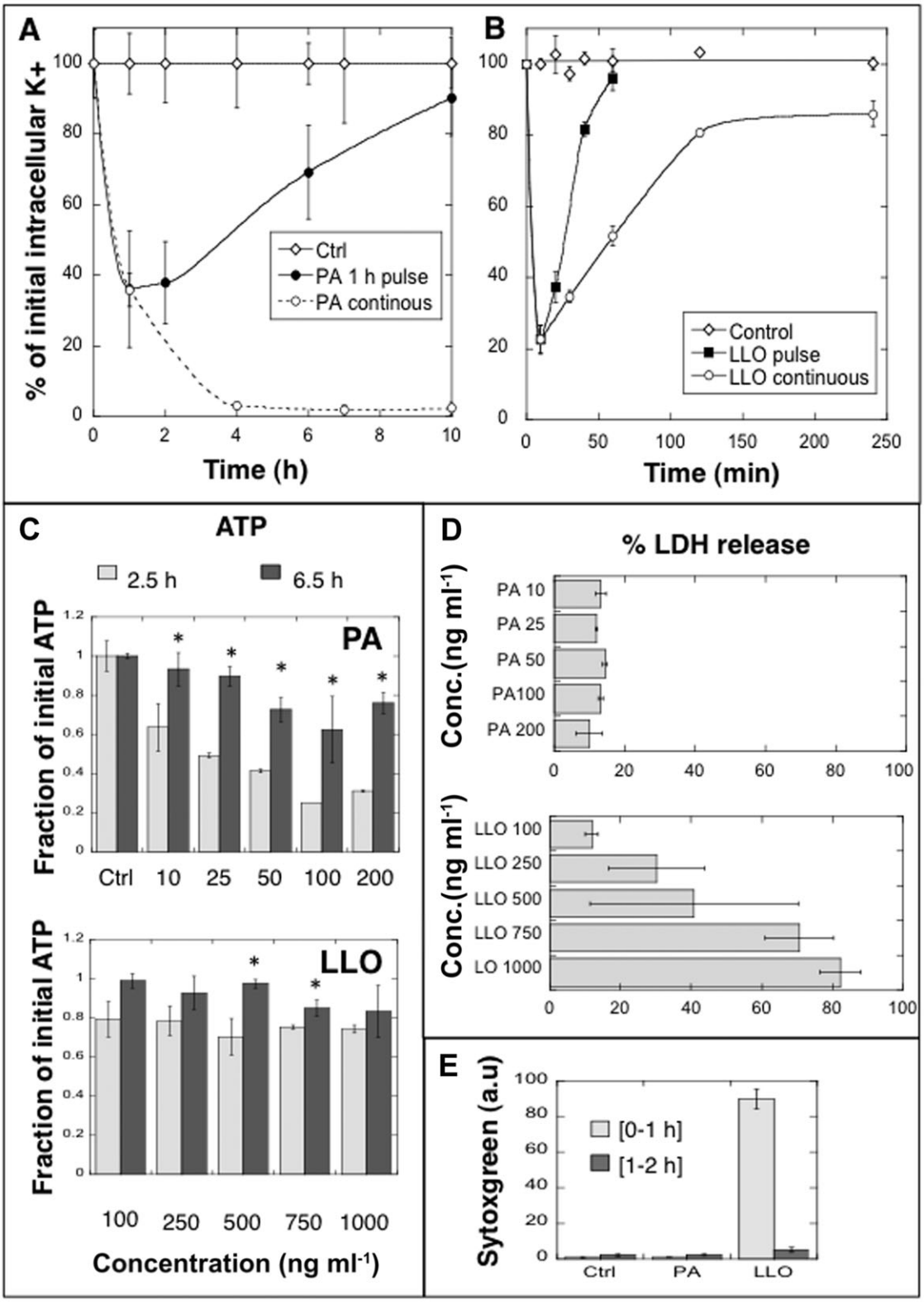
A
% of initial intracellular K+
Ctrl
PA 1 h pulse
PA continous
Time (h)
B
Control
LLO pulse
LLO continuous
Time (min)
C
ATP
2.5 h
6.5 h
PA
Fraction of initial ATP
Ctrl 10 25 50 100 200
LLO
Concentration (ng ml-1)
D
% LDH release
Conc.(ng ml-1)
PA 10
PA 25
PA 50
PA100
PA 200
LLO 100
LLO 250
LLO 500
LLO 750
LO 1000
E
Sytoxgreen (a.u)
[0-1 h]
[1-2 h]
Ctrl
PA
LLO

Fig. 1. Permeabilization of HT29 cells by aerolysin and LLO.
A. HT29 cells in six-well plates were treated with 10 ng ml^{-1} proaerolysin (PA) for 1 h (solid line) or continuously (dashed line). The intracellular potassium content was determined as a function of time by flame photometry ($n = 3$, errors bars represent standard deviations).
B. Cells in six-well plates were treated with 500 ng ml^{-1} LLO for 10 min (black squares) or continuously (white circles) ($n = 3$, errors bars represent standard deviations).
C. Cells in 96-well plates were submitted to different concentrations of proaerolysin for 1 h followed by 5.5 h of recovery or to different concentrations of LLO concentration in continuous for 6.5 h. The amount of LDH released in the medium was measured using a membrane integrity assay kit.
D. Cells in six-well plates were treated with 10 ng ml^{-1} proaerolysin or 500 ng ml^{-1} LLO for 1 h. At time 0 or 1 h post intoxication 1 μM SytoxGreen was added to the cells for 1 h. SytoxGreen-positive cells were measured by flow cytometry and the data were analysed using FlowJo.
E. Cellular ATP level was measured at 2.5 and 6.5 h after proaerolysin and LLO treatment as in (C). Note that LDH and ATP assays were performed in 96-well plates and thus the toxin concentrations cannot be linearly transposed to the potassium efflux assays performed in six-well plates. *Statistical significant differences, $p < 0.05$.

which could provide an explanation for the rapid recovery of cells following exposure to LLO. Cells however also replenish their intracellular potassium pool following exposure to the related, but pH-insensitive, toxin perfringolysin O (PFO) (Fig. S1D), in agreement with previous findings (Walev *et al*., 2001).

Interestingly, recovery of intracellular potassium levels following exposure to either PA^{pulse} or LLO did not require *de novo* protein synthesis as shown by the lack of effect of the protein synthesis inhibitor cycloheximide (Fig. S1E and F).

To further probe the extent of cellular ion homeostasis recovery, we measured the cellular ATP content 2.5 and 6.5 h after PA^{pulse} and LLO treatment. For PA^{pulse}-treated cells, ATP levels were still low after 2.5 h but restored back to > 80% of controls after 6.5 h (Fig. 1C, top panel). While for LLO-treated cells close to full recovery was already observed after 2.5 h (Fig. 1C, bottom panel).

LLO-induced plasma membrane lesions are transient

In agreement with the literature on CDCs (Walev *et al*., 2001), the LLO pores formed in HT29 cells were very large, allowing the passage of the 140 kDa enzyme lactate dehydrogenase (LDH) (Fig. 1D, bottom panel). The presence of these large plasma membrane pores was however transient, again in agreement with previous observations (Walev *et al*., 2001). This was shown by incubating LLO-treated HT29 cells with the DNA-intercalating agent SytoxGreen (900 Da) either during the first or during the second hour following toxin treatment. While SytoxGreen could penetrate into the cells during the first hour, it remained excluded during the second (Fig. 1E), revealing the recovery of plasma membrane integrity. Neither LDH release (Fig. 1D, top panel) nor SytoxGreen staining (Fig. 1E) was observed for PA^{pulse}-treated cells, consistent with the established small size of the pore (diameter of 1.5–2 nm).

Altogether, these experiments show that aerolysin forms small pores that do not allow the passage of LDH, nor of the 900 Da SytoxGreen probe but allow the passage of small ions such as potassium. When exposure to proaerolysin is transient (PA^{pulse}), HT29 cells can recover their cytosolic K+ and ATP levels after about 8 h. LLO leads to the formation of large pores that allow the passage of ions as well as proteins such as LDH. This striking change in plasma membrane permeability is however transient and cell recover their normal K+ and ATP levels within less than 2 h.

PFT-induced activation of the p38 and ERK MAP kinases promotes recovery of intracellular K+ levels

The fact that recovery of cellular potassium following exposure to PFTs is independent of protein synthesis (Fig. S1E and F) shows that repair is not under translational control, and thus must depend on signalling via pre-existing proteins. As a first unbiased approach, we used commercially available Human phospho-kinase arrays, which harbour 46 kinase antibodies against 29 different kinases. Cells were treated or not with LLO or PA^{pulse} for 1 h. As an additional control, cells were treated with a mutant proaerolysin – Y221G – which is able to bind to cells and multimerize but fails to insert into the membrane to form pores (Tsitrin *et al*., 2002). The response was remarkably specific, and similar for both toxins (Fig. 2A and B). Phosphorylation was observed for the MAP kinases p38 – as previously reported for *Staphylococcus* alpha-haemolysin, streptolysin O, pneumolysin O, anthrolysin O and Cry5B, a member of the pore-forming Crystal toxin family (Ratner *et al*., 2006; Aguilar *et al*., 2009 and reviewed in Porta *et al*., 2010) – and for JNK, as reported for pneumolysin O (Aguilar *et al*., 2009). In addition we found that both PA and LLO trigger activation of ERK. MEK1/2 – the kinases upstream from ERK, MSK – a common target of p38 and ERK (Vermeulen *et al*., 2009) – and CREB – the first identified MSK substrate (Vermeulen *et al*., 2009) were also activated by both toxins (Fig. 2A and B). The activation of MAPKs was not due to a possible contamination of the toxin preparations with LPS, since treatment with polymyxin B

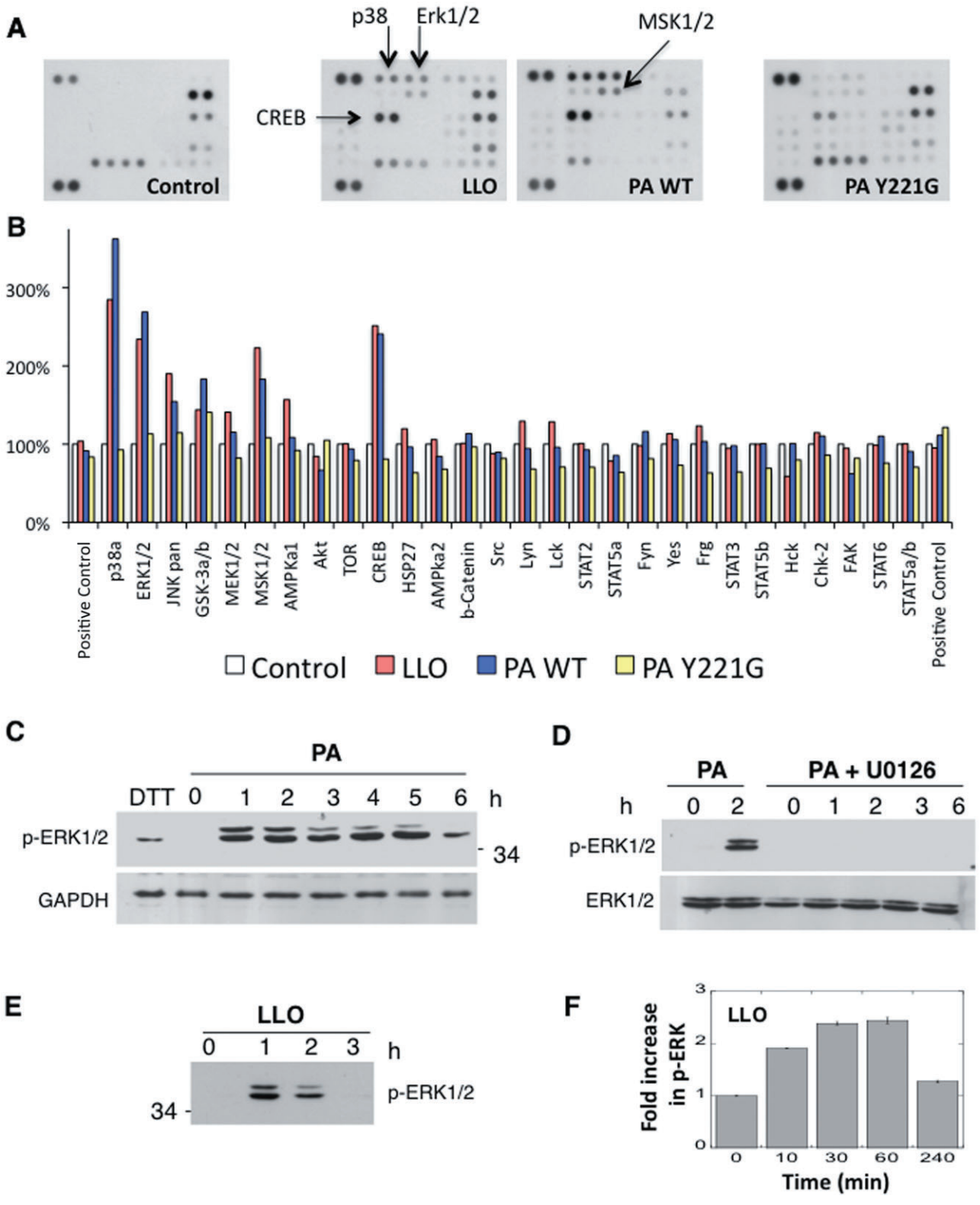
A
p38
Erk1/2
MSK1/2
CREB
Control
LLO
PA WT
PA Y221G
B
300%
200%
100%
0%
Positive Control
p38a
ERK1/2
JNK pan
GSK-3a/b
MEK1/2
MSK1/2
AMPKa1
Akt
TOR
CREB
HSP27
AMPKa2
b-Catenin
Src
Lyn
Lck
STAT2
STAT5a
Fyn
Yes
Frg
STAT3
STAT5b
Hck
Chk-2
FAK
STAT6
STAT5a/b
Positive Control
Control
LLO
PA WT
PA Y221G
C
PA
DTT 0 1 2 3 4 5 6 h
p-ERK1/2
34
GAPDH
D
PA
PA + U0126
h 0 2 0 1 2 3 6
p-ERK1/2
ERK1/2
E
LLO
0 1 2 3 h
34
p-ERK1/2
F
LLO
Fold increase in p-ERK
3
2
1
0
0 10 30 60 240
Time (min)

Fig. 2. PFT-induced kinase activation.
A and B. HT29 in six-well plates were treated with 500 ng ml^{-1} LLO, 10 ng ml^{-1} PA or Y221G for 1 h. Phosphorylation of protein kinases was analysed with a human phospho-kinase profiler array. Membranes were exposed to films (A) as well as scanned and dots intensities were quantified using a Typhoon (B). Values represent the mean of the doublets observed on the arrays. Only one of the two membranes of the kinase array is shown for each condition since no toxin-induced changes were observed on the second part of the array. In (B), results were normalized to the no toxin control.
C. HT29 cells cultured in six-well plates were treated with 10 ng ml^{-1} proaerolysin for 1 h and further incubated in toxin-free medium for different times. Western blots were performed using an antibody against phosphorylated ERK.
D. Cells were pre-treated with 10 μM MEK1 inhibitor U0126 for 1 h prior to PA treatment. Cells were subject to 1 h pulse of 10 ng ml^{-1} PA, fresh U0126 was added during the recovery time.
E. Cells were treated with 500 ng ml^{-1} LLO continuously for different times.
F. Quantification of phospho-ERK induction by LLO treatment.

did not modify the activation pattern revealed by the phospho-arrays (not shown). Using similar arrays, we also found that the phosphorylation pattern was not modified when chelating extracellular calcium with 5 mM EGTA, nor by inhibiting caspases – and in particular caspase-1 – using the pan-caspase inhibitor zVAD (not shown). We had previously shown that proaerolysin triggers the activation of caspase-1 in HeLa and Chinese Hamster Ovary (CHO) cells following a 3 h exposure to PA (Gurcel *et al.*, 2006). We here found that caspase-1 is also activated in HT29 cells by PA after 3 h and by LLO after 1 h (not shown).

P38 and ERK activation by PA^{pulse} and LLO were confirmed using SDS-PAGE and Western blotting. Activation indeed occurred in response to both toxins and was transient (Fig. 2C, E and F, Fig. S2). Activation of ERK1/2 occurred via its upstream kinase MEK1/2 since the MEK1/2 inhibitor U0126 prevented PA-induced ERK activation (Fig. 2D).

We next investigated whether the activation of the MAP kinase pathways was important for the recovery of cellular ion homeostasis. Cells were treated either with a p38 inhibitor (SB203580), a MEK inhibitor (U0126), or both, or with a JNK inhibitor (SP600125). The inhibitors did not affect the kinetics of proaerolysin or LLO-induced K+ efflux (Fig. S3B and C). Inhibition of either p38 or ERK however significantly impaired the recovery of intracellular K+ following pore formation by PA^{pulse} or LLO, and the effect was additive (Fig. 3), consistent with the idea that these two pathways act in parallel to promote recovery of ion homeostasis. In contrast, the JNK inhibitor had no effect (Fig. S3D and E). Future studies are needed to understand how MAP kinases are activated and how they promote the recovery of ion homeostasis.

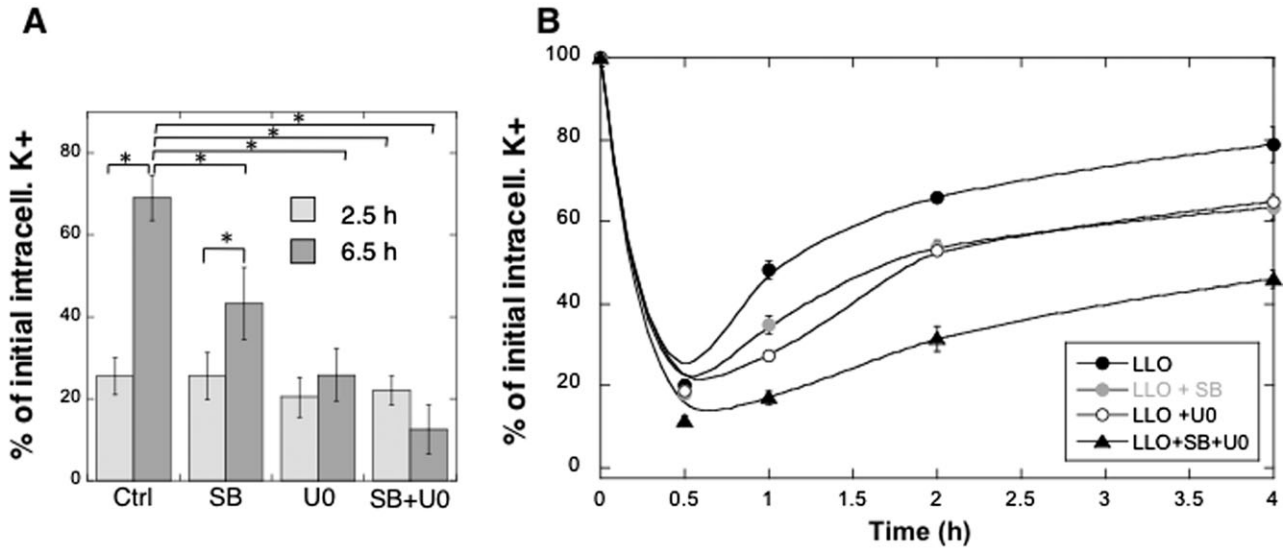

Fig. 3. Cellular potassium recovery after PFTs injury depends on p38 and ERK.
A. HT29 cells in six-well plates were pre-treated for 1 h with p38 inhibitor SB203580 (10 μM), MEK-1 inhibitor U0126 (10 μM) or both together. Cells were treated with 10 ng ml^{-1} PA for 1 h followed by recovery in toxin-free medium containing fresh drugs.
B. HT29 cells were pre-treated with SB203580, U0126 or both together before addition of 500 ng ml^{-1} LLO. Intracellular potassium was measured at the indicated times. *Statistical significant differences, $p < 0.05$.

PFT-induced K+ efflux triggers autophagy

It has been shown recently that, in addition to MAP kinases activation, certain PFTs – *Vibro cholerae* cytolysin (Gutierrez *et al*., 2007), *Staphylococcus* alpha-haemolysin (Kloft *et al*., 2010; Mestre *et al*., 2010) and LLO (Meyer-Morse *et al*., 2010) – also trigger autophagy. We here extend this list to proaerolysin (Fig. 4A, Fig. S4A). We found that proaerolysin triggers the conjugation of the LC3 with phosphatidyl ethanolamine (PE), revealed by the conversion of LC3 I to LC3 II (Fig. 4A, Fig. S4A), a hallmark of autophagy (Klionsky *et al*., 2008), and by the appearance of LC3-GFP-positive structures in proaerolysin-treated cells (Fig. S4B). Conversion of LC3 I to LC3 II was dependent upon Atg5, a gene required for autophagy (Cecconi and Levine, 2008), since it no longer occurred in fibroblasts derived from Atg5 knockout mice (Mizushima *et al*., 2001) (Fig. 4A).

To investigate whether autophagy plays a role in the restoration of ion homeostasis, we tested the effect of the autophagy inhibitor 3-methyl adenine (3-MA). 3-MA did not alter the recovery of intracellular potassium in HT29 cells following exposure to either PA^{pulse} or LLO (Fig. S4C and D) suggesting that autophagy does not promote membrane repair. It has been proposed for *Vibrio* cytolysin that autophagy may promote the degradation of the pore (Gutierrez *et al*., 2007). To investigate this possibility, we monitored the kinetics of degradation of the aerolysin heptamer in HT29. We found that level of heptamers remained stable over the 6 h period of the experiment (Fig. S4E), consistent with the remarkable stability of the pore forming complex (Lesieur *et al*., 1999), but ruling out a role for autophagy in the degradation of the aerolysin pore. This observation also indicates that HT29 cells do not eliminate the pores via exosomes, as proposed for staphylococcal alpha-haemolysin (Husmann *et al*., 2009). Why cells trigger autophagy in response to PFTs is therefore unclear.

It has been observed in yeast that during nutrient starvation, cells enter a quiescent state and that autophagy is part of this programme, allowing recycling of cytosolic constituents (Smets *et al*., 2010; Yang and Klionsky, 2010). In analogy, we raised the possibility that mammalian cells enter a quiescent-like state upon pore formation to remain in a minimal energy consumption state while plasma membrane repair takes place. The importance of autophagy in cell survival would then correlate with the time required for plasma membrane repair: following PA^{pulse}, when recovery is very slow, autophagy would contribute to cell survival; in contrast following exposure to LLO, when recovery is very fast, autophagy would not be important. To test this possibility, we again made use of the $atg5^{-/-}$ Mouse Embryonic Fibroblasts (MEFs). PFTs concentrations were sought that allowed MEFs to recover their intracellular potassium

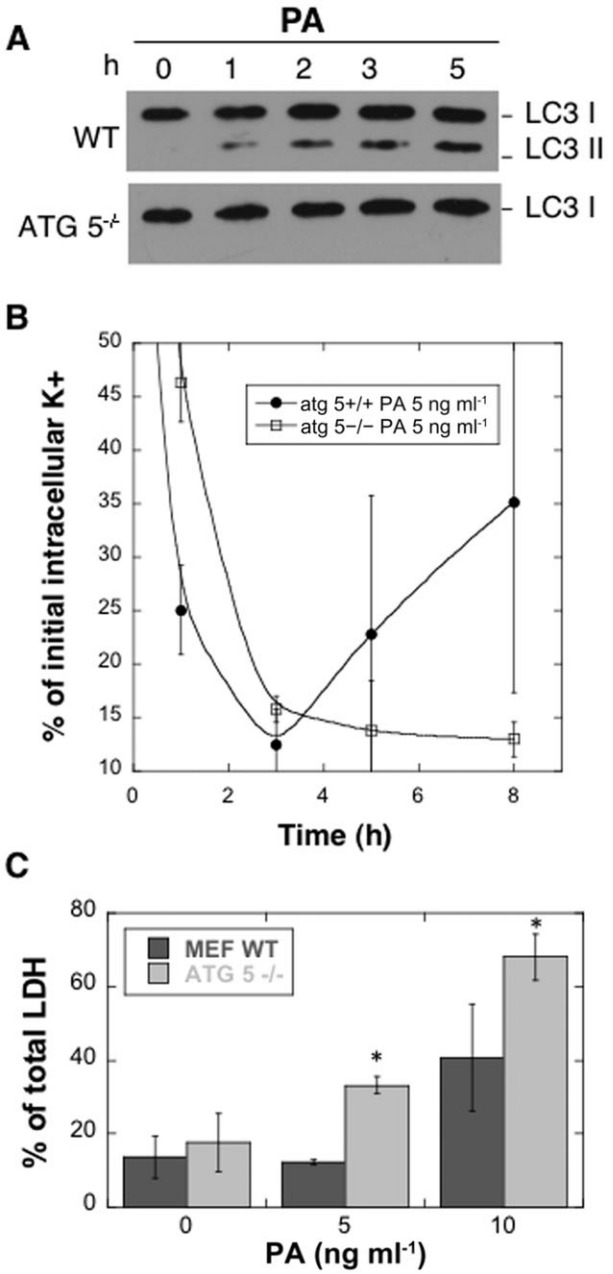

Fig. 4. Autophagy promotes cell survival in response to aerolysin.
A. Mouse Embryonic Fibroblasts (MEFs) from control and $atg5^{-/-}$ mice were treated with 20 ng ml^{-1} proaerolysin for 1 h and cell extracts were analysed by SDS-PAGE and Western blotting against LC3.
B. Control and $atg5^{-/-}$ MEFs were cultured in six-well plates and treated with 5 and 3.5 ng ml^{-1} proaerolysin, respectively, for 1 h and subsequently incubated in toxin fee medium. Intracellular potassium was measured at the indicated times.
C. Control and $atg5^{-/-}$ MEFs were cultured in 96-well plates and treated with different concentration of proaerolysin for 6 h and cell death was monitored by LDH release.

levels at the population level, at least to some extent (Fig. 4B for PA, Fig. S4F for LLO). When MEFs were exposed to 100 ng ml^{-1} LLO, whether during 10 min or continuously, potassium levels recovered to controls levels within less than 2 h, irrespective of the presence of ATG5 (Fig. S4F), in agreement with the lack of effect of 3-MA observed on LLO-treated Atg5$^{-/-}$ cells (Fig. S4D). When control MEFs were exposed to 5 ng ml^{-1} PA^{pulse}, potassium levels dropped during the first 3 h, followed by a slow partial recovery (Fig. 4B). When Atg5$^{-/-}$ cells were treated with a lower concentration PA^{pulse} (3.5 ng ml^{-1}), recovery of K+ at 3 h was no longer observed (Fig. 4B). The apparent discrepancy with the lack of effect of 3-MA on PA-treated HT29 cells is probably due to the fact that potassium efflux and recovery occur more rapidly in HT29 cells, and thus in these cells, as upon LLO treatment, autophagy is not necessary. Since LDH does not cross aerolysin pores (Fig. 1C), we next used LDH release as a readout for PA-induced cell death and found that death was increased in the absence of atg5 (Fig. 6F).

Altogether, these observations indicate that autophagy is not *per se* required for the membrane repair. However, if membrane repair is a very slow process, as observed for certain toxins in certain cell types (such as PA in MEFs), then plasma membrane repair fails, probably via a secondary effect.

PFTs trigger a transient arrest in proteins synthesis

To further investigate the possibility that plasma membrane permeabilization triggers the transition to a quiescent-like state, we analysed whether arrest in protein synthesis – a hallmark of quiescence – occurred upon exposure to PFTs. HT29 cells were submitted to a PA^{pulse} and 2, 4.5 and 7 h after toxin addition, newly synthesized proteins were labelled by incubating cells for 20 min with ^{35}S-Cys/Met. Strikingly, 2 h after toxin addition, protein synthesis dropped by 80%, an effect that was not observed with the Y221G mutant (Fig. 5A). After longer times, synthesis resumed reaching control levels at ≈ 7 h (Fig. 5A). This recovery was not observed when cells where continuously exposed to proaerolysin (Fig. S5A). The PA^{pulse}-induced drop in protein synthesis did not lead to a drop in mRNA synthesis (not shown) in agreement with the fact that we have previously observed a three- to fourfold increase in the mRNAs of HMG-CoA reductase and fatty acid synthase in PA-treated cells (Gurcel *et al.*, 2006). A similar drop in protein synthesis upon exposure to PA or LLO was observed in Retinal Pigmented Epithelial (RPE1) cells (Fig. S6B).

A direct consequence of the PFT-induced arrest of protein synthesis should be the apparent downregulation of short-lived proteins. We therefore analysed the effect of proaerolysin on the cellular levels of the proto-oncogene myc, which has a half-life of ~30 min (Hann and Eisenman, 1984). Myc levels drastically dropped upon a PA^{pulse} but gradually recovered to reach control levels after ≈ 7 h (Fig. 7B), a recovery that was not observed upon continuous exposure to PA (Fig. S5B). Disappearance of myc could be blocked by the proteasome inhibitor MG132 (Fig. 5C). Similarly Myc level transiently dropped upon treatment of HT29 cells with LLO, an effect that was blocked by MG132 (Fig. 5D and E). The transient arrest of protein synthesis in response to PFTs is independent of the activation of the MAP kinases or of caspase-1, since p38 and ERK inhibitors (Fig. S5C and D) or the pan-caspase inhibitor zVAD (not shown).

It has been shown that Cry PFTs trigger the unfolded protein response (UPR) in *Caenorhabditis elegans* in a p38-dependent manner (Bischof *et al.*, 2008). It is also well established that the PERK arm of the UPR triggers an arrest in the general protein synthesis (Ron and Walter, 2007). The fact that we did not observed any effect of p38 inhibitors on the PA-induced arrest in proteins synthesis suggest that arrest does not occur via the UPR. To address this issue more directly, we performed RNAi again the three transmitters of the UPR: PERK, IRE1 and ATF6 (Ron and Walter, 2007), in RPE1 cells, which are amenable to efficient transfection. While silencing was efficient, LLO- and PA^{pulse}-induced arrests in protein synthesis were not affected (Fig. S6) indicating that the UPR is not involved.

One established pathway leading to arrest in protein synthesis is the phosphorylation of eukaryotic initiation factor 2 alpha (eIF2α) (Holcik and Sonenberg, 2005). Under resting conditions, eIF2α is not phosphorylated and is part of the complex that recruits the initiator Met-tRNA to the start codon. When phosphorylated however, it acts as an inhibitor of general translation. We found that proaerolysin and LLO trigger a pronounced but transient phosphorylation of eIF2α (Fig. S7A–C) – as also found for staphylococcal alpha-haemolysin during the course of this study (Kloft *et al.*, 2010). It is therefore possible that eIF2α phosphorylation may play a role in PFT-induced arrest in protein synthesis but other factors, such as low ATP levels, likely also play an important in reducing protein synthesis. We indeed found that PA still triggers an arrest in protein synthesis in MEF expressing a point mutant of eIF2α that cannot be phosphorylated (Costa-Mattioli *et al.*, 2007) (not shown).

PFTs trigger the formation of lipid droplets

Finally it is well known that starvation in yeast has a strong impact on lipid metabolism (Zhang *et al.*, 2010) and in particular triggers the formation of lipid droplets (Willison and Johnston, 1985), a dynamic lipid storage organelles observed in all eukaryotic cells (Beller *et al.*, 2010). We therefore investigated whether PFTs trigger the formation of lipid droplets. Within 1–3 h of toxin treatment, an

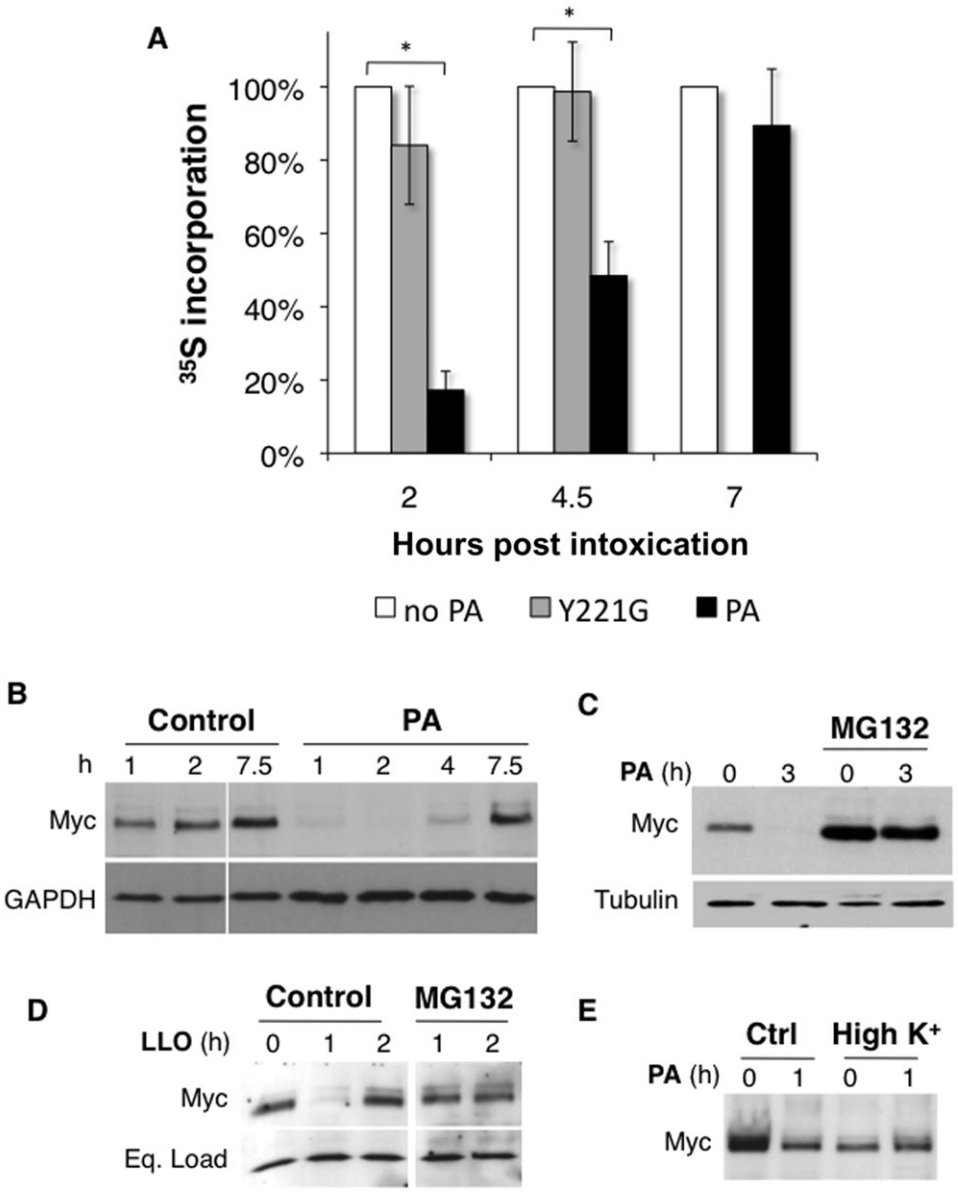

Fig. 5. Aerolysin and LLO lead to a transient arrest in protein synthesis.
A. HT29 cells cultured in 10 cm dishes were treated with 10 ng ml^{-1} WT or Y221G mutant proaerolysin for 1 h and ^{35}S-methionine incorporation was monitored after different time points. Cell extracts were analysed by SDS-PAGE followed by Coomassie blue staining and autoradiography (A). The radioactivity in each lane was quantified in three independent experiments (B). Errors bars represent the standard deviation.
B. HT29 cells were treated with 10 ng ml^{-1} PA for 1 h and the level of myc protein was monitored by Western blotting (50 μg protein per lane) over time.
C. HT29 cells were pre-treated with proteasome inhibitor MG132 (10 μM) before exposure to 10 ng ml^{-1} proaerolysin. Cell extracts were analysed by SDS-PAGE and Western blotting against myc.
D. HT29 cells were pre-treated with proteasome inhibitor MG132 (10 μM) before exposure to 500 ng ml^{-1} LLO. The level of myc was analysed as above.

increase of lipid droplets could be observed both by fluorescence microscopy, using the neutral lipid marker Bodipy 493/503 (Fig. 6A and C), and by electron microscopy (Fig. 6B). A similar increase in the number of lipid droplets was observed when treating cells with LLO, the related toxin SLO (streptolysin O) as well as with staphylococcal alpha-haemolysin (Fig. 6D), but not with the Y221G aerolysin mutant (Fig. 6C). PA^{pulse}-induced lipid droplet formation was not inhibited by silencing PERK, ATF6 or IRE1 in RPE1 cells (not shown) indicating that the UPR is not involved in this process. We also tested whether lipid droplet formation was MAP kinase-dependent and found

that while the p38 inhibitor had no effect, both MEK (U0126) and ERK2 (Ste-MEK1$_{13}$) inhibitors abolished PA-induced droplet formation (Fig. 6E). Finally, we analysed whether droplet formation was beneficial to the cells. A moderate but significant increase in cell death was observed upon PA^{pulse} treatment when cells were incubated with Triacsin C, an inhibitor of lipid droplets that blocks long-chain acyltransferase activity (Igal *et al*., 1997) (Fig. 6F).

Intracellular potassium is a central regulator of the cellular responses to PFTs

We previously found that PFT-induced changes in potassium concentration led to the activation of caspase-1 (Gurcel *et al*., 2006). We therefore wondered whether changes in cytoplasmic potassium would influence the various PFT-induced cellular responses described in this study. Efflux of potassium was prevented by incubating cells in a high K+ buffer and thus abolishing the potassium gradient across the plasma membrane. We checked that high extracellular potassium did not lead to a drop of cellular ATP (not shown) and did not affect pore formation by aerolysin and LLO (Fig. S8). Remarkably we found that high extracellular potassium prevented PA-induced p38 activation (Fig. 7A), erk activation (Fig. 7B), eIF2α activation (Fig. S7D), conversion of LC3 I into LC3 II (Fig. 7C), arrest in protein synthesis – interestingly it had been observed in the 1960s that potassium concentrations affect *in vitro* protein synthesis (Lubin and Ennis, 1964) – as revealed by the constant level of Myc (Fig. 7D) as well as the formation of lipid droplets (Fig. 7E).

That K+ efflux from cells is not only necessary but sufficient to trigger these events was shown using the potassium ionophore nigericin, which triggered p38 (Fig. 7F), erk (Fig. 7G) and eIF2α (Fig. S6E) activation, as well as LC3 conversion (Fig. 7H). From this analysis, cellular potassium therefore emerges as one of the master regulators of the cellular response to PFTs.

Discussion

The aim of this study was to obtain a more comprehensive view of cellular responses to PFTs. We chose two toxins – aerolysin and LLO – that differ in terms of structure, receptors, pores size and stability/lifetime. We first confirmed that these two toxins indeed generate lesions of different sizes and showed that the integrity of the plasma membrane is restored with $\approx$ 1 h – at the population level – for the large LLO pores and only after $>$ 6 h for the smaller aerolysin pores. The inverse correlation between pore size and ability of cells to repair their plasma membrane indicates that pore number or pore stability/lifetime are more important in terms of recovery than pore size.

It is quite remarkable that cells can loose 80% of their cellular potassium, and yet fully recover, especially since, in conjunction with the potassium loss, other ion gradients between the inside and the outside of the cell are almost undoubtedly affected. The second unexpected finding is that the recovery of the ion homeostasis, which is probably subsequent or concomitant to the recovery of membrane integrity, does not require *de novo* protein synthesis, even in the case of aerolysin-treated cells where the process takes several hours. This indicates that cells mobilize existing protein networks to repair their plasma membrane and restore the ion balance.

We found that a large number of pathways are activated by PFTs – and the list is probably not exhaustive – highlighting the complexity of the response. The response was however specific since out of the 29 kinases represented on the phospho-arrays, only six were significantly activated by proaerolysin and LLO (Fig. 2A and B). Furthermore, both toxins triggered the same signalling cascades. This suggests that, as least for the pathways analysed here, the initiating event is the disruption of plasma membrane integrity and the ensuing change in cellular ion composition. This hypothesis is supported by the fact that incubating cells in a high-potassium medium (either by inverting the extracellular Na+ and K+ ratios or by adding K+ to the tissue culture medium) prevented the activation of every single pathway reported here, as well as of the caspase-1-SREBP axis that we have previously described (Gurcel *et al*., 2006). Also the potassium ionophore nigericin was able to activate each of the studied pathway. It therefore appears that either cells have K+ sensing devices or potassium efflux triggers changes that the cell can detect and respond to.

We propose to categorize the signalling response pathways activated by PFTs into four groups (Fig. 8), which would act in parallel but on different timescales. The first is related to the immune response. It includes the activation of the inflammasome and its downstream targets (Gurcel *et al*., 2006; Dunne *et al*., 2010) and modulation of the expression of inflammatory genes for example through the dephosphorylation of histones (Hamon *et al*., 2007). The second category of pathways comprises signalling routes that do not require any gene transcription to operate in full. These include toxin-induced endocytosis and exocytosis (Idone *et al*., 2008; Husmann *et al*., 2009; Tam *et al*., 2010), the MAP kinase pathways and possibly the inhibition of host protein SUMOylation recently described for LLO and other CDCs (Ribet *et al*., 2010). One hypothesis is that these pathways ensure that the plasma membrane integrity and the ionic balance are restored, a process that is ATP-dependent. Since these events require several hours for certain toxins, the third category of signalling cascades leads the cell into a quiescent, low-energy-consumption state: protein translation

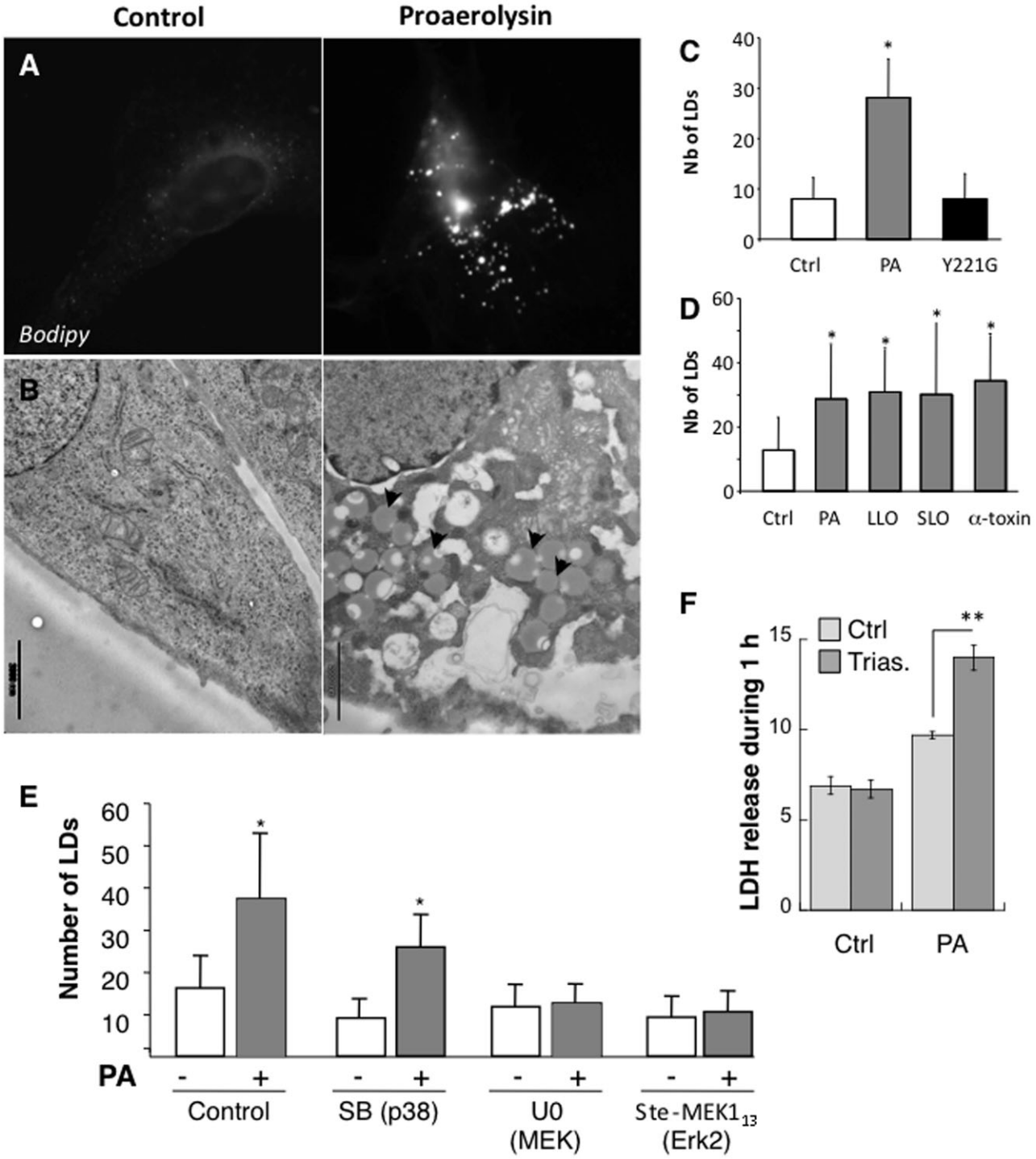

is arrested, cytosolic constituents are recycled via autophagy and energy is stored in lipid droplets. This third category is systematically activate upon plasma membrane permeabilization. Its impact on cell viability however depends and correlates with the time required to repair the toxin-induced damage. Finally a fourth category involves signalling routes leading to transcription, the effect of which would only kick in once protein synthesis has resumed. It is also possible that translation of specific messengers already occurs during the bulk protein synthesis arrest, as observed during the Unfolded Protein Response (Ron and Walter, 2007). This fourth category includes the SREBP pathway (Gurcel *et al*., 2006) and the modulation of gene expression through the dephosphory-

Fig. 6. PFTs induce lipid droplet formation.
A. Fluorescent microscopy on HeLa cells, cultured on glass cover slides in six-well plates, is treated with 2 ng ml^{-1} PA for 3 h in continuous and stained with the neutral lipid binding dye Bodipy493/503.
B. Electron microscopy on Chinese Hamster Ovary (CHO) cells treated with 10 ng ml^{-1} PA for 3 h.
C. Quantification of lipid droplets (LDs) in HeLa cells treated with 2 ng ml^{-1} PA or Y221G for 3 h. LDs were stained using Bodipy493/503 and observed by fluorescent microscopy. The acquired images were deconvoluted using the Huygens software before LDs analysis and quantification were performed with the Metamorph software. Errors bars represent standard deviations of 50–60 cells.
D. Quantification of LDs in HeLa cells after 3 h of PA (2 ng ml^{-1}), LLO (500 ng ml^{-1}), SLO (250 ng ml^{-1}) or *Staphylococcus aureus* α-toxin (1 mg ml^{-1}).
E. Quantification of LDs in HeLa cells treated with 2 ng ml^{-1} PA for 3 h preceded by 1 h pre-treatment with p38 inhibitor 203580 (10 μM), MEK-1 inhibitor U0126 (10 μM) or ERK2 inhibitor Ste-MEK1$_{13}$ (10 μM).
F. HT29 cell in six-well plates are pre-treated for 1 h with 1 μM Triacsin C prior intoxication. Cell were subsequently incubated with PA 10 ng ml^{-1} for 1 h followed by 6 h in a toxin-free medium, always in the presence of Triacsin C. Released LDH was then measured.

lation of histones (Hamon *et al*., 2007). Cleary multiple levels of cross-talk probably operate between these various pathways. A straight forward example would be that the arrest of protein synthesis will lead to the depletion of short-lived molecules such as Myc – without affecting long-lived molecules, and this might impact on the signalling events of category 2.

This study, in combination with the existing literature, illustrates the complexity of the cellular responses to PFTs and how much remains to be understood. One interesting open question concerns the mechanisms that lead to recovery of plasma membrane integrity. While it is clear that changes in cellular ion composition are the trigger of signalling cascades, it is equally clear that the pathways that are eventually successful in restoring the plasma membrane integrity are different between different toxins/mechanical damage since membrane repair occurs on quite different timescales: seconds for mechanical breaches; minutes for LLO type pores, hours for aerolysin types pores (Bischofberger *et al*., 2009). The mechanisms that operate in each of these cases have not fully been elucidated (for review see Bischofberger *et al*., 2009). It is however not surprising that a lipid line lesion is repaired by different mechanism than a protein lined lesion. Why the mechanisms differ between LLO and aerolysin is however less apparent and will be the topic of further investigation. Since aerolysin and LLO bind to different receptors, putative removal of the toxin from the cell surface could occur via different routes with different kinetics. It has been proposed that PFO pores are rapidly endocytosed via a calcium-activated endocytic mechanism (Idone *et al*., 2008) and that membrane repair also requires calcium-triggered lysosomal exocytosis (Tam *et al*., 2010). Our observations however indicate that even in the absence of extracellular calcium, plasma membrane integrity can be restored after transient exposure to LLO or PA, supporting the existence of multiple repair pathways.

A second, even more interesting open question, is how cells sense the action of PFTs. The initiating event for the here-described responses is clearly the breach in plasma membrane integrity – which also occurs during mechanical disruption of cellular membranes (McNeil and Kirchhausen, 2005). Our observation that high extracellular potassium prevents the onset set of multiple signalling cascades suggests that cells are equipped with devices that directly or indirectly sense changes in ion concentrations. While it is well known that cells can sense intracellular ion concentrations such as calcium, less is know about the more 'housekeeping' ion, potassium. Moreover, we cannot fully rule out that potassium leakage triggers subsequent events, and that these are the ones actually sensed by the cells. Considering the importance of repairing plasma membrane damage in a variety of cellular contexts, linked to disease or normal function, understanding how cells sense plasma membrane damage is of great general scientific interest.

Experimental procedures

Cells and reagents

HT29 cells were grown in RPMI media supplemented with 10% fetal calf serum, 1% penicillin-streptomycin and 1% glutamine (all from Gibco) in a humidified incubator with 5% CO_2 at 37°C. HeLa cells were cultured in MEM media supplemented with 10% fetal calf serum, 1% penicillin-streptomycin, 1% glutamine and 1% NEAA. RPE1 cells and MEFs from wild-type or atg5 knockout mice were cultured in DMEM media supplemented with 10% fetal calf serum, 1% penicillin-streptomycin and 1% glutamine.

High-potassium medium was composed of 5 mM NaCl, 140 mM KCl, 10 mM Hepes, 1.3 mM $CaCl_2$, 0.5 mM $MgCl_2$, 0.36 mM K_2HPO_4, 0.44 mM KH_2PO_4, 5.5 mM D-glucose, 4.2 mM $NaHCO_3$. WT and mutant aerolysin Y221G were purified as described (Buckley *et al*., 1981). PA was produced in *Aeromonas salmonicida* as previously described (Buckley, 1990). LLO was produced in *Escherichia coli* and purified as described (Hamon *et al*., 2007). Anti-phospho p38 and total p38 antibody were from Cell Signaling Technology, antibodies against eIF2α phosphorylated at serine 51 and anti-total eIF2α from Biosource. SB203580, Ste-MEK1$_{13}$ and Nigericin were purchased from Calbiochem. U0126 was from Cell Signaling technology, zVAD-fmk was from Bachem. SytoxGreen and Bodipy493/503 were from Invitrogen. Triacsin C was from BioMol. Polymyxin B was from Sigma

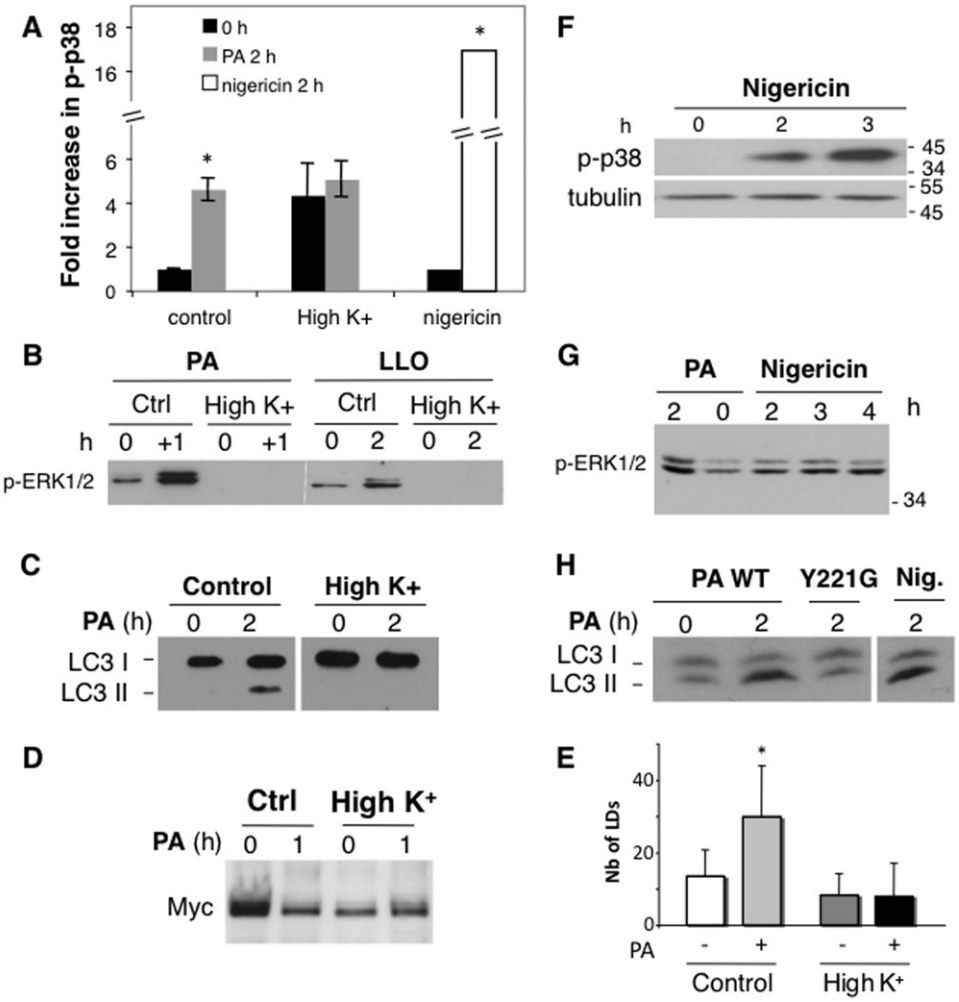

Fig. 7. Inhibition of potassium efflux inhibits PFT-induced cellular response pathways.
A. HT29 cells were treated continuously with 20 ng ml^{-1} proaerolysin in normal or high-potassium media. Activation of p38 was monitored by Western blotting ($n = 3$).
B. ERK phosphorylation in HT29 was monitored after PA (10 ng ml^{-1}, pulse 1 h followed by recovery 1 h) or LLO (500 ng ml^{-1}, continuous 2 h) treatment in high-potassium media.
C. Control MEFs were treated with proaerolysin (20 ng ml^{-1}) in normal or high-potassium medium. Cell extracts (50 μg protein per lane) were then analysed by SDS-PAGE and Western blotting against LC3.
D. HT29 cells treated with 10 ng ml^{-1} PA for 1 h in normal or high-potassium medium. Levels of myc were analysed by Western blotting.
E. Quantification of LDs was performed in HeLa cells after treatment with 2 ng ml^{-1} PA for 3 h in control medium or high-potassium buffer.
F. HT29 cells were treated with 10 μM nigericin for the indicated times and analysed for p38 phosphorylation.
G. HT29 cells were treated with 10 μM nigericin for the indicated times and analysed for ERK phosphorylation.
H. Control MEFs were treated either with the inactive Y221G aerolysin mutant or with nigericin (10 μM) and the conversion of LC3 was analysed by Western blotting. *Statistical significant differences, $p < 0.05$.

Western blot analysis

Equal numbers of cells ($4{\cdot}10^5$ per ml for HT29 and $2{\cdot}10^5$ per ml for HeLa) were seeded in plates to achieve ~70% confluence after 72 h for HT29 and 48 h for HeLa. Cells were treated as indicated and washed once with PBS at 4°C before being lysed at 4°C for 20 min in radioimmune precipitation buffer [150 mM NaCl, 50 mM Tris-HCl (pH 7.2), 1% Triton X-100, 1% Sodium deoxycholate, 0.05% SDS, 4 mM $NaVO_4$, 5 mM EGTA and protease inhibitors]. Pre-cleared lysats (10 min at 13 000 r.p.m.) were subjected to SDS-PAGE and Western blotting using the relevant antibody. Band intensities were quantified using ImageJ software (NIH).

Phospho-array analysis

Phospho-array was performed using a Human Phospho-Kinase Array kit from R&D systems (ATY003). HT29 cells were seeded ($4{\cdot}10^5$ per ml) in six-well plate 72 h before experiment. The assay was performed according to the manufacture protocol, 250 μg of protein lysate was used per membrane. Dot intensities were scanned and quantified using a Typhoon.

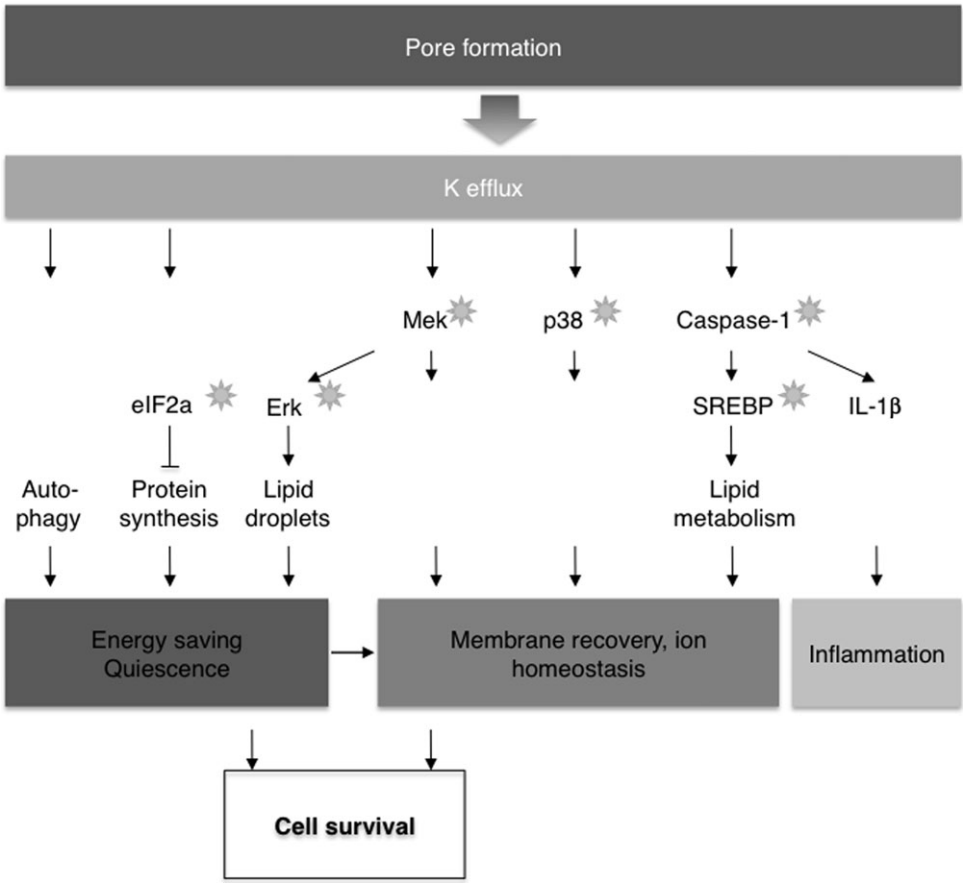

Fig. 8. Schematic representation of the cellular responses to PFTs. PFTs lead to the decreased of cellular potassium levels. This in turn leads to the activation of a variety of signalling cascades that can be categorized based on their putative purpose. Autophagy, arrest in protein synthesis and lipid droplet formation reveal the entry of PFT-damaged cells into a quiescent, low-energy-consumption, state. MAP kinase pathways promote the recovery of plasma membrane integrity and of ion balance. A third set of pathways trigger inflammation and modulate the immune response.

Potassium efflux, ATP, LDH and SytoxGreen staining measurements

For potassium efflux measurements confluent cells in six-well plates were treated or not with the required drugs for 1 h before adding the toxins for different times. At specific time points the cells were washed three times on ice with cold, potassium-free choline buffer (Abrami *et al*., 1998b). The cells were then lysed in choline buffer containing 0.5% Triton X-100 for at least 30 min at room temperature under constant shaking. The lysats were analysed with a M401 flame photometer equipped with a potassium filter from Sherwood (UK) using pure propane gas.

ATP was measured using the CellTiter-Glo Luminescent Cell Viability Assay (Promega). LDH release was measured following the instructions of the CytoTox-One Homogeneous Membrane integrity Assay kit (Promega). SytoxGreen staining, to estimate cell death, was performed by 10 min in the CO_2 incubator at concentration of 1 μM. Cells were then analysed on a CyAn ADP fluorescence-activated cell sorter (FACS) from Dako Cytomation and data processed using FlowJo 6.4 software.

Metabolic labelling

Cells were incubated for 30 min in cysteine/methionine free Dulbecco's modified Eagle's medium (DMEM) (Invitrogen), followed by a 20 min labelling at 37°C in DMEM supplemented with 70 μCi ml^{-1} ^{35}S-methionine/cysteine (Hartman Analytics). Cells were washed three times with RPMI prior to protein extraction. Radioactive samples were separated on SDS-PAGE (12.5%), proteins were fixed with an acetate–[2-propanol]–water (10/25/65, v/v/v) solution. Radioactive signal was amplified with Amplify™ Fluographic Reagent (Amersham Bioscience) and measured using a Typhoon (Amersham Bioscience). Band intensities were quantified using Typhoon quantification software.

Lipid droplets quantification

HeLa cells ($2{\cdot}10^5$ per ml) were seeded in six-well plates containing glass coverslips to achieve ~70% confluence after 48 h. Cells were washed three times with PBS, fixed with PBS containing 3% PFA and lipid droplets were stained using Bodipy493/503. Images were acquired using an Axiovert 200M fluorescent microscope containing an AxioCam MRm and the AxioVison (Rel. 4.8)

software. Images were deconvoluted using Huygens software before lipid droplets analysis and quantification with the Metamorph software.

Electron microscopy

After 2-day growth and toxin treatment, confluent CHO cells were fixed with 2.5% EM grade glutaraldehyde. Cells were washed with 0.1 M cacodylate buffer, stained with 2% uranyl acetate, deshydratated with EtOH and embedding in LX112 Epon.

Accession numbers

Aerolysin: P09167, AERA_AERHY.
Listeriolysin O: P13128, TACY_LISMO.

Acknowledgements

We kindly thank Pascale Cossart (Institut Pasteur) for providing the LLO plasmid as well as some purified toxin, Noboru Mizushima for providing us with Atg5$^{-/-}$ MEFs, Komla Sobo (University of Geneva) for the HT29 cells. F.G.v.d.G. is an international Fellow of the Howard Hughes Medical Institute. B.F. was a recipient of a fellowship from the Fondation pour la Recherche Médicale, M.B. is a recipient of an iPhD SystemsX.ch fellowship.

References

Abrami, L., Fivaz, M., Decroly, E., Seidah, N.G., François, J., Thomas, G., *et al*. (1998a) The pore-forming toxin proaerolysin is processed by furin. *J Biol Chem* **273:** 32656–32661.

Abrami, L., Fivaz, M., Glauser, P.-E., Parton, R.G., and van der Goot, F.G. (1998b) A pore-forming toxin interact with a GPI-anchored protein and causes vacuolation of the endoplasmic reticulum. *J Cell Biol* **140:** 525–540.

Abrami, L., Fivaz, M., and van Der Goot, F.G. (2000) Adventures of a pore-forming toxin at the target cell surface. *Trends Microbiol* **8:** 168–172.

Aguilar, J.L., Kulkarni, R., Randis, T.M., Soman, S., Kikuchi, A., Yin, Y., and Ratner, A.J. (2009) Phosphatase-dependent regulation of epithelial mitogen-activated protein kinase responses to toxin-induced membrane pores. *PLoS ONE* **4:** e8076.

Aroian, R., and van der Goot, F.G. (2007) Pore-forming toxins and cellular non-immune defenses (CNIDs). *Curr Opin Microbiol* **10:** 57–61.

Beller, M., Thiel, K., Thul, P.J., and Jackle, H. (2009) Lipid droplets: a dynamic organelle moves into focus. *FEBS Lett* **584:** 2176–2182.

Bellier, A., Chen, C.S., Kao, C.Y., Cinar, H.N., and Aroian, R.V. (2009) Hypoxia and the hypoxic response pathway protect against pore-forming toxins in *C. elegans*. *PLoS Pathog* **5:** e1000689.

Bhakdi, S., and Tranum-Jensen, J. (1991) Alpha-toxin of *Staphylococcus aureus*. *Microbiol Rev* **55:** 733–751.

Bischof, L.J., Kao, C.Y., Los, F.C., Gonzalez, M.R., Shen, Z., Briggs, S.P., *et al*. (2008) Activation of the unfolded protein response is required for defenses against bacterial pore-forming toxin *in vivo*. *PLoS Pathog* **4:** e1000176.

Bischofberger, M., Gonzalez, M.R., and van der Goot, F.G. (2009) Membrane injury by pore-forming proteins. *Curr Opin Cell Biol* **21:** 589–595.

Buckley, J.T. (1990) Purification of cloned proaerolysin released by a low protease mutant of *Aeromonas salmonicida*. *Biochem Cell Biol* **68:** 221–224.

Buckley, J.T., Halasa, L.N., Lund, K.D., and MacIntyre, S. (1981) Purification and some properties of the hemolytic toxin aerolysin. *Can J Biochem* **59:** 430–435.

Cecconi, F., and Levine, B. (2008) The role of autophagy in mammalian development: cell makeover rather than cell death. *Dev Cell* **15:** 344–357.

Chopra, A.K., Xu, X., Ribardo, D., Gonzalez, M., Kuhl, K., Peterson, J.W., and Houston, C.W. (2000) The cytotoxic enterotoxin of *Aeromonas hydrophila* induces proinflammatory cytokine production and activates arachidonic acid metabolism in macrophages. *Infect Immun* **68:** 2808–2818.

Costa-Mattioli, M., Gobert, D., Stern, E., Gamache, K., Colina, R., Cuello, C., *et al*. (2007) eIF2alpha phosphorylation bidirectionally regulates the switch from short- to long-term synaptic plasticity and memory. *Cell* **129:** 195–206.

Dunne, A., Ross, P.J., Pospisilova, E., Masin, J., Meaney, A., Sutton, C.E., *et al*. (2010) Inflammasome activation by adenylate cyclase toxin directs Th17 responses and protection against *Bordetella pertussis*. *J Immunol* **185:** 1711–1719.

Gilbert, R.J. (2010) Cholesterol-dependent cytolysins. *Adv Exp Med Biol* **677:** 56–66.

Golstein, P., and Kroemer, G. (2007) Cell death by necrosis: towards a molecular definition. *Trends Biochem Sci* **32:** 37–43.

Gonzalez, M.R., Bischofberger, M., Pernot, L., van der Goot, F.G., and Freche, B. (2008) Bacterial pore-forming toxins: the (w)hole story? *Cell Mol Life Sci* **65:** 493–507.

Gray, J.V., Petsko, G.A., Johnston, G.C., Ringe, D., Singer, R.A., and Werner-Washburne, M. (2004) 'Sleeping beauty': quiescence in *Saccharomyces cerevisiae*. *Microbiol Mol Biol Rev* **68:** 187–206.

Gurcel, L., Abrami, L., Girardin, S., Tschopp, J., and van der Goot, F.G. (2006) Caspase-1 activation of lipid metabolic pathways in response to bacterial pore-forming toxins promotes cell survival. *Cell* **126:** 1135–1145.

Gutierrez, M.G., Saka, H.A., Chinen, I., Zoppino, F.C., Yoshimori, T., Bocco, J.L., and Colombo, M.I. (2007) Protective role of autophagy against *Vibrio cholerae* cytolysin, a pore-forming toxin from *V. cholerae*. *Proc Natl Acad Sci USA* **104:** 1829–1834.

Hadders, M.A., Beringer, D.X., and Gros, P. (2007) Structure of C8alpha-MACPF reveals mechanism of membrane attack in complement immune defense. *Science* **317:** 1552–1554.

Hamon, M.A., Batsche, E., Regnault, B., Tham, T.N., Seveau, S., Muchardt, C., and Cossart, P. (2007) Histone modifications induced by a family of bacterial toxins. *Proc Natl Acad Sci USA* **104:** 13467–13472.

Hann, S.R., and Eisenman, R.N. (1984) Proteins encoded by the human c-myc oncogene: differential expression in neoplastic cells. *Mol Cell Biol* **4:** 2486–2497.

Heuck, A.P., Moe, P.C., and Johnson, B.B. (2010) The cholesterol-dependent cytolysin family of gram-positive bacterial toxins. *Subcell Biochem* **51:** 551–577.

Holcik, M., and Sonenberg, N. (2005) Translational control in stress and apoptosis. *Nat Rev Mol Cell Biol* **6:** 318–327.

Huffman, D.L., Abrami, L., Sasik, R., Corbeil, J., van der Goot, F.G., and Aroian, R.V. (2004) Mitogen-activated protein kinase pathways defend against bacterial pore-forming toxins. *Proc Natl Acad Sci USA* **101:** 10995–11000.

Husmann, M., Dersch, K., Bobkiewicz, W., Beckmann, E., Veerachato, G., and Bhakdi, S. (2006) Differential role of p38 mitogen activated protein kinase for cellular recovery from attack by pore-forming *S. aureus* alpha-toxin or streptolysin O. *Biochem Biophys Res Commun* **344:** 1128–1134.

Husmann, M., Beckmann, E., Boller, K., Kloft, N., Tenzer, S., Bobkiewicz, W., *et al*. (2009) Elimination of a bacterial pore-forming toxin by sequential endocytosis and exocytosis. *FEBS Lett* **583:** 337–344.

Iacovache, I., Paumard, P., Scheib, H., Lesieur, C., Sakai, N., Matile, S., *et al*. (2006) A rivet model for channel formation by aerolysin-like pore-forming toxins. *EMBO J* **25:** 457–466.

Iacovache, I., van der Goot, F.G., and Pernot, L. (2008) Pore formation: an ancient yet complex form of attack. *Biochim Biophys Acta* **1778:** 1611–1623.

Idone, V., Tam, C., Goss, J.W., Toomre, D., Pypaert, M., and Andrews, N.W. (2008) Repair of injured plasma membrane by rapid Ca^{2+}-dependent endocytosis. *J Cell Biol* **180:** 905–914.

Igal, R.A., Wang, P., and Coleman, R.A. (1997) Triacsin C blocks *de novo* synthesis of glycerolipids and cholesterol esters but not recycling of fatty acid into phospholipid: evidence for functionally separate pools of acyl-CoA. *Biochem J* **324** (Part 2)**:** 529–534.

Kennedy, C.L., Smith, D.J., Lyras, D., Chakravorty, A., and Rood, J.I. (2009) Programmed cellular necrosis mediated by the pore-forming alpha-toxin from *Clostridium septicum*. *PLoS Pathog* **5:** e1000516.

Kepp, O., Galluzzi, L., Zitvogel, L., and Kroemer, G. (2010) Pyroptosis – a cell death modality of its kind? *Eur J Immunol* **40:** 627–630.

Klionsky, D.J., Abeliovich, H., Agostinis, P., Agrawal, D.K., Aliev, G., Askew, D.S., *et al*. (2008) Guidelines for the use and interpretation of assays for monitoring autophagy in higher eukaryotes. *Autophagy* **4:** 151–175.

Kloft, N., Busch, T., Neukirch, C., Weis, S., Boukhallouk, F., Bobkiewicz, W., *et al*. (2009) Pore-forming toxins activate MAPK p38 by causing loss of cellular potassium. *Biochem Biophys Res Commun* **385:** 503–506.

Kloft, N., Neukirch, C., Bobkiewicz, W., Veerachato, G., Busch, T., von Hoven, G., *et al*. (2010) Pro-autophagic signal induction by bacterial pore-forming toxins. *Med Microbiol Immunol* **199:** 299–309.

Korchev, Y.E., Bashford, C.L., Pederzolli, C., Pasternak, C.A., Morgan, P.J., Andrew, P.W., and Mitchell, T.J. (1998) A conserved tryptophan in pneumolysin is a determinant of the characteristics of channels formed by pneumolysin in cells and planar lipid bilayers. *Biochem J* **329** (Part 3)**:** 571–577.

Lesieur, C., Frutiger, S., Hughes, G., Kellner, R., Pattus, F., and van Der Goot, F.G. (1999) Increased stability upon heptamerization of the pore-forming toxin aerolysin. *J Biol Chem* **274:** 36722–36728.

Lubin, M., and Ennis, H.L. (1964) On the role of intracellular potassium in protein synthesis. *Biochim Biophys Acta* **80:** 614–631.

McNeil, P.L., and Kirchhausen, T. (2005) An emergency response team for membrane repair. *Nat Rev Mol Cell Biol* **6:** 499–505.

McNeil, P.L., and Steinhardt, R.A. (2003) Plasma membrane disruption: repair, prevention, adaptation. *Annu Rev Cell Dev Biol* **19:** 697–731.

Mestre, M.B., Fader, C.M., Sola, C., and Colombo, M.I. (2010) Alpha-hemolysin is required for the activation of the autophagic pathway in *Staphylococcus aureus*-infected cells. *Autophagy* **6:** 110–125.

Meyer-Morse, N., Robbins, J.R., Rae, C.S., Mochegova, S.N., Swanson, M.S., Zhao, Z., *et al*. (2010) Listeriolysin O is necessary and sufficient to induce autophagy during *Listeria monocytogenes* infection. *PLoS ONE* **5:** e8610.

Mizushima, N., Yamamoto, A., Hatano, M., Kobayashi, Y., Kabeya, Y., Suzuki, K., *et al*. (2001) Dissection of autophagosome formation using Apg5-deficient mouse embryonic stem cells. *J Cell Biol* **152:** 657–668.

Nelson, K.L., Brodsky, R.A., and Buckley, J.T. (1999) Channels formed by subnanomolar concentrations of the toxin aerolysin trigger apoptosis of T lymphomas. *Cell Microbiol* **1:** 69–74.

Porta, H., Cancino-Rodezno, A., Soberon, M., and Bravo, A. (2011) Role of MAPK p38 in the cellular responses to pore-forming toxins. *Peptides* **32:** 601–606.

Ratner, A.J., Hippe, K.R., Aguilar, J.L., Bender, M.H., Nelson, A.L., and Weiser, J.N. (2006) Epithelial cells are sensitive detectors of bacterial pore-forming toxins. *J Biol Chem* **281:** 12994–12998.

Ribet, D., Hamon, M., Gouin, E., Nahori, M.A., Impens, F., Neyret-Kahn, H., *et al*. (2010) *Listeria monocytogenes* impairs SUMOylation for efficient infection. *Nature* **464:** 1192–1195.

Ron, D., and Walter, P. (2007) Signal integration in the endoplasmic reticulum unfolded protein response. *Nat Rev Mol Cell Biol* **8:** 519–529.

Rosado, C.J., Buckle, A.M., Law, R.H., Butcher, R.E., Kan, W.T., Bird, C.H., *et al*. (2007) A common fold mediates vertebrate defense and bacterial attack. *Science* **317:** 1548–1551.

Schuerch, D.W., Wilson-Kubalek, E.M., and Tweten, R.K. (2005) Molecular basis of listeriolysin O pH dependence. *Proc Natl Acad Sci USA* **102:** 12537–12542.

Shepard, L.A., Shatursky, O., Johnson, A.E., and Tweten, R.K. (2000) The mechanism of pore assembly for a cholesterol-dependent cytolysin: formation of a large prepore complex precedes the insertion of the transmembrane beta-hairpins. *Biochemistry* **39:** 10284–10293.

Smets, B., Ghillebert, R., De Snijder, P., Binda, M., Swinnen, E., De Virgilio, C., and Winderickx, J. (2010) Life in the midst of scarcity: adaptations to nutrient availability in *Saccharomyces cerevisiae*. *Curr Genet* **56:** 1–32.

Tam, C., Idone, V., Devlin, C., Fernandes, M.C., Flannery, A., He, X., *et al*. (2010) Exocytosis of acid sphingomyelinase by wounded cells promotes endocytosis and plasma membrane repair. *J Cell Biol* **189:** 1027–1038.

Tsitrin, Y., Morton, C.J., El Bez, C., Paumard, P., Velluz, M.C., Adrian, M., *et al*. (2002) Conversion of a transmembrane to

a water-soluble protein complex by a single point mutation. *Nat Struct Biol* **9:** 729–733.
Vermeulen, L., Berghe, W.V., Beck, I.M., De Bosscher, K., and Haegeman, G. (2009) The versatile role of MSKs in transcriptional regulation. *Trends Biochem Sci* **34:** 311–318.
Walev, I., Palmer, M., Martin, E., Jonas, D., Weller, U., Hohn, B.H., *et al*. (1994) Recovery of human fibroblasts from attack by the pore-forming alpha-toxin of *Staphylococcus aureus*. *Microb Pathog* **17:** 187–201.
Walev, I., Bhakdi, S.C., Hofmann, F., Djonder, N., Valeva, A., Aktories, K., and Bhakdi, S. (2001) Delivery of proteins into living cells by reversible membrane permeabilization with streptolysin-O. *Proc Natl Acad Sci USA* **98:** 3185–3190.
Willison, J.H., and Johnston, G.C. (1985) Ultrastructure of *Saccharomyces cerevisiae* strain AG1-7 and its responses to changes in environment. *Can J Microbiol* **31:** 109–118.
Yang, Z., and Klionsky, D.J. (2010) Mammalian autophagy: core molecular machinery and signaling regulation. *Curr Opin Cell Biol* **22:** 124–131.
Yarovinsky, T.O., Monick, M.M., Husmann, M., and Hunninghake, G.W. (2008) Interferons increase cell resistance to Staphylococcal alpha-toxin. *Infect Immun* **76:** 571–577.
Zhang, J., Vemuri, G., and Nielsen, J. (2010) Systems biology of energy homeostasis in yeast. *Curr Opin Microbiol* **13:** 382–388.

Supporting information

Additional Supporting Information may be found in the online version of this article:

Fig. S1. Recovery of potassium in proaerolysin-, LLO- and PFO-treated cells.
A. HT29 cells in six-well plates were treated with 10 ng ml^{-1} proaerolysin for 1 h before recovery in toxin-free medium or in continuous. Cells were counted 7 h post intoxication.
B. HT29 cells in six-well plates were treated with 1 mM EGTA and 10 ng ml^{-1} PA for 1 h followed by recovery in toxin-free medium containing fresh EGTA. Intracellular potassium was measured at the indicated times.
C. HT29 cell in six-well plates were treated with 1 mM EGTA and 500 ng ml^{-1} LLO for 10 min followed by recovery in toxin and EGTA-free medium.
D. HT29 cells in six-well plates were treated with 500 ng ml^{-1} PFO for 10 min or in continuous.
E and F. Cells were pre-treated with 10 μg ml^{-1} cycloheximide (CHX) 1 h prior to and during toxin treatment. PA was used at 10 ng ml^{-1} for 1 h and LLO at 500 ng ml^{-1} in continuous.
Fig. S2. P38 MAPK is activated upon PFTs treatment.
A. HT29 cells cultured in six-well plates were treated with 10 ng ml^{-1} proaerolysin for 1 h and further incubated in toxin-free medium for different times. Protein quantification was performed prior to SDS-PAGE and equal amounts of total protein were loaded in each lane (50 μg per lane). Western blotting was performed against phosphorylated p38 MAPK. α-Tubulin was used as a loading marker.
B. Three independent experiments of (A) were used and quantified to realize the plot.
C. HT29 cells were treated continuously with WT or Y221G mutant proaerolysin (20 ng ml^{-1}) or LLO (100 ng ml^{-1}). Cell extracts were analysed as in (A).
D. HT29 cells were treated with 500 ng ml^{-1} LLO in continuous. Samples were analysed using phospho-arrays at different times. Preliminary experiments indicated that the signal peaks at 30 min.
Fig. S3. P38 and MEK inhibitors do not affect pore formation by proaerolysin and LLO.
A. HT29 cells cultured in six-well plates are treated with p38 inhibitor SB203580 (10 μM), MEK-1 inhibitor U0126 (10 μM) or both. No efflux of potassium was observed in the absence of toxin.
B and C. HT29 cells cultured in six-well plates were pre-treated for 1 h with SB203580 and U0126 prior to addition of 10 ng ml^{-1} PA or 500 ng ml^{-1} LLO. Intracellular potassium concentrations were measured at the indicated times.
D and E. HT29 cells were pre-treated for 1 h with JNK inhibitor SP600125 (10 μM) prior to treatment with 10 ng ml^{-1} PA for 1 h or with 500 ng ml^{-1} LLO in continuous.
Fig. S4. Potassium recovery is independent of the autophagy machinery.
A. HeLa and HT29 cells were cultured in six-well plates and treated continuously with 20 ng ml^{-1} proaerolysin for 2 h. Cell extracts (50 μg protein per lane) were analysed by SDS-PAGE and Western blotting against LC3. During autophagy, the LC3 protein is conjugated with a PE moiety, leading to the LC3-II formation, which has a shifted electrophoretic mobility.
B. HeLa cells were transiently transfected with GFP-LC3. Treatment of these cells with aerolysin induced GFP-LC3 targeting to punctuated structures.
C and D. HT29 cells in six-well plates were pre-treated for 1 h with autophagy inhibitor 3-MA (5 mM). Cells were then treated with 10 ng ml^{-1} proaerolysin for 1 h or 500 ng ml^{-1} LLO for 10 min, followed by recovery in toxin-free medium containing fresh drugs. Intracellular potassium was measured at the indicated times.
E. HT29 cells in six-well plates were treated with 10 ng ml^{-1} proaerolysin for 1 h before recovery in a toxin-free medium. Total-cell extract was analysed by Western blotting with an antibody against aerolysin to reveal the toxin heptamer.
F. Control and atg5$^{-/-}$ MEFs were treated with 100 ng ml^{-1} LLO in continuous or for 10 min followed by recovery in fresh medium. Intracellular potassium was over time.
Fig. S5. Proaerolysin induces inhibition in protein translation is independent of MAPKs.
A. HT29 cells in 10 cm dishes were treated with 20 ng ml^{-1} proaerolysin continuously and ^{35}S-methionine incorporation was monitored after different time points.
B. HT29 cells in six-well plates were treated with 10 ng ml^{-1} proaerolysin for 1 h followed by recovery in toxin-free medium or in continuous. The level of myc protein was monitored by Western blotting (50 μg protein per lane) and showed recovery only in pulse condition.
C and D. HT29 cells cultured in six-well plates were pre-treated with p38 inhibitor 203580 (10 μM), MEK-1 inhibitor U0126 (10 μM) or both inhibitors together followed by 10 ng ml^{-1} proaerolysin treatment for 1 h. ^{35}S-methionine incorporation was monitored 2 and 4.5 h post intoxication. Cell extracts were analysed by SDS-PAGE (50 μg protein per lane) followed by Coomassie blue staining and autoradiography. The radioactivity in each lane was quantified using a Typhoon™.

Fig. S6. PFT-induced arrest in protein synthesis is independent of the Unfolded Protein Response.

A. The efficiency of Qiagen-validated siRNA duplexes in silencing PERK, Ire1 and ATF6 after 72 h in RPE1 cells was tested by qPCR.

B. RPE1 cells in which PERK, Ire1 and ATF6 cultured in six-well dishes were treated with proaerolysin (20 and 40 ng ml^{-1}) or with LLO (500 or 1000 ng ml^{-1}) for 1 h. After 1 h of toxin treatment, ^{35}S-methionine was incorporated for 20 min. Cell extracts were run on an SDS gel and the total radioactivity per lane was quantified using a Typhoon™ scanner.

Fig. S7. eIF2α is activated upon cellular exposure to PFTs.

A. HT29 cells were treated with 10 ng ml^{-1} proaerolysin for 1 h and further incubated in toxin-free medium for different times. Western blots were performed using an antibody against phosphorylated eIF2α. Total eIF2α protein level was used as a loading control.

B. Three independent experiments of (A) were used and quantified to realize the plot.

C. HT29 cells were treated continuously with WT or Y221G mutant proaerolysin (20 ng ml^{-1}) or LLO (100 ng ml^{-1}) for 2 h in continuous.

D. HT29 cells were treated continuously with 20 ng ml^{-1} proaerolysin in normal or high-potassium media. Activation of eIF2α was monitored by Western blotting on three independent experiments ($n = 3$).

E. HT20 cells were treated with 10 μM nigericin for the indicated times and analysed for eIF2α phosphorylation.

Fig. S8. High extracellular potassium does not affect aerolysin- and LLO-induced haemolysis. Human erythrocytes were resuspended in either Hank (5 mM K+) or Inverted Hank buffer (140 mM K+), followed by toxin treatment in 96-well plates. PA (1250 ng ml^{-1}, A) or LLO (156 ng ml^{-1}, B) were added to diluted erythrocytes, and incubated at 37°C. Data were collected at a wavelength of 600 nm every 11 s until reaction completed using a SpectraMax Pro 5 microplate reader.

Please note: Wiley-Blackwell are not responsible for the content or functionality of any supporting materials supplied by the authors. Any queries (other than missing material) should be directed to the corresponding author for the article.